JOURNAL OF CATALYSIS **168,** 421–430 (1997)
ARTICLE NO. CA971671

Surface Characterization of Zirconia-Coated Alumina and Silica Carriers

S. Damyanova,*[,1] P. Grange,† and B. Delmon†

*Institute of Catalysis, Bulgarian Academy of Science, 1113 Sofia, Bulgaria; and †Université Catholique de Louvain, Unité de Catalyse et Chimie de Matériaux Divisés, Place Croix du Sud, 2/17, 1348 Louvain-la-Neuve, Belgium

Received October 7, 1996; revised January 23, 1997; accepted January 23, 1997

Silica- and alumina-supported zirconia samples have been prepared by impregnation of the supports with a solution of zirconium alkoxide (*n*-propoxide) in *n*-propanol containing ZrO_2 in the ranges 1.2–28.6 and 2.2–23.2 wt%, respectively. The samples were characterized by the S_{BET} method, XRD, XPS, and FTIR. The x-ray diffraction showed that zirconia on silica was amorphous for all concentrations of ZrO_2. Zirconia on alumina was amorphous up to 17.1 wt% ZrO_2; beyond this value crystallites were formed. The increase in the XPS IZr 3*d*/ISi 2*p* indicates that ZrO_2 appears as a monolayer on silica near the theoretical monolayer coverage (about 28.6 wt%), whereas for alumina-supported zirconia samples the monolayer is formed at lower ZrO_2 content (between 12.9 and 17.1 wt%). It was observed by pyridine adsorption that the strong Lewis acid sites on alumina decreased after deposition of zirconia. However, the number of Lewis acid sites on silica-supported zirconia samples, evoked by an increase of the positive charge on Zr atoms compared to pure zirconia, increases with increasing ZrO_2 content. Some Brønsted acid sites were detected on ZrO_2/SiO_2 samples due to the slightly higher electron density on the oxygen associated with Si atoms detected by XPS.

1. INTRODUCTION

Zirconium oxide has received considerable attention as a catalyst for various reactions including hydrogenation of hydrocarbons (1–3), cracking (4), dehydrogenation (5, 6), hydrodesulphurization (7), etc. This specific behaviour of zirconium oxide in these reactions is due to a special combination of surface properties, namely the preservation of both acidic and basic sites, on the one hand, and reducing and oxidizing properties, on the other (8–10). Recently, the enhancement of the acidic properties of zirconia by addition of sulphate ions led to a new generation of solid catalysts with superacid properties (10–15). Zirconium oxide is also interesting as a support. It might even become more important as a catalyst support material than as a catalyst (16, 17). For instance, Rh supported on ZrO_2 exhibits higher catalytic activity for hydrogenation of CO and CO_2, compared with Rh supported on Al_2O_3 and SiO_2 (16).

However, zirconia has a low specific surface area and it is more expensive than the traditional oxide materials such as alumina and silica. Because of these two reasons, the object of research in the past few years has been the stabilization of highly dispersed zirconium oxide on a high surface area support. Dispersed zirconium oxide on alumina and silica could constitute a new class of attractive carriers, because they would combine the unique chemical properties of ZrO_2 with the high surface area and mechanical stability of the supports.

Some studies concerning the preparation and surface properties of ZrO_2/SiO_2 and ZrO_2/Al_2O_3 binary oxides have been reported (18, 19). It has been shown that the standard impregnation of silica or alumina with an aqueous solution of zirconium nitrate led to the formation of large ZrO_2 particles which left a considerable part of the support uncovered (18, 19). One alternative method for avoiding the formation of large ZrO_2 particles is the control of zirconium alkoxide hydrolysis by addition of acetylacetone molecules bound to the zirconium atoms (19–23). The reactivity of zirconium alkoxide towards hydrolysis is substantially reduced due to the formation of a complex compound with acetylacetone. But it is not yet clear whether a very high dispersion of zirconium at the surface of silica or alumina can be achieved.

To our knowledge, our work is the first attempt to investigate whether the deposition of ZrO_2 on silica and alumina can lead to the formation of a zirconia monolayer. The work concentrates on: (i) the effect of the type of the support on the morphology and dispersion of zirconia; (ii) the interaction between zirconia and the support, and (iii) the influence of the zirconia content. The samples were characterized using atomic absorption, specific surface area measurements, x-ray diffraction (XRD), x-ray photoelectron spectroscopy (XPS), and Fourier transformed infrared spectroscopy (FTIR) adsorption of pyridine.

2. EXPERIMENTAL

2.1. Sample Preparation

The alumina and silica supports were first calcined at 773 K for 8 h before the introduction of zirconium. The

[1] E-mail: banchem@bgearn.acad.bg.

0021-9517/97 $25.00

supports were added to a solution of a known amount of zirconium *n*-propoxide in *n*-propanol. The mixture was stirred for 4 h at room temperature under inert atmosphere to avoid air–moisture contact. After this the *n*-propanol was removed by evaporation in a Rotavapor at 333 K. The resulting solid was exposed to air overnight to facilitate the hydrolysis of $Zr(n\text{-}OC_3H_7)_4$. The samples were dried at 383 K for 12 h and calcined in air at 773 K for 7 h. Some samples were calcined at 973 K for 7 h. The ZrO_2 content in the ZrO_2/Al_2O_3 and ZrO_2/SiO_2 samples were in the ranges 2.2–23.2 and 1.2–28.6 wt%, respectively. The maximum content of ZrO_2 corresponds to a theoretical monolayer coverage of ZrO_2 on the corresponding supports. For comparison, a mechanical mixture ($SiO_2 + 10$ wt% ZrO_2) was prepared and calcined at 773 K for 7 h.

2.2. Characterization

The elemental analyses (Al, Si, Zr) were performed by inductively coupled plasma-atomic emission spectroscopy (ICP-AES).

The specific surface areas and pore volume of the samples were measured by the BET method with a Micromeritics model ASAP 2000 using nitrogen at 77 K. Prior to measurements, all the samples were outgassed for 4 h at 423 K.

The x-ray diffraction patterns were recorded using a Siemens D-5000 powder diffractometer with nickel-filtered Cu $K\alpha$ radiation ($\alpha = 1.5404$ Å). The step-scans were taken over the range of 2θ from 20 to 70° in steps of 0.015°, the intensity data for each being collected for 5 s.

The x-ray photoelectron spectra were obtained with a Surface Science Instruments SSX-100 model 206 spectrometer with a monochromatised Al $K\alpha$ source, operating at 10 kV and 12 mA. The residual pressure inside the analysis chamber was below 5×10^{-9} Torr (1 Torr = 133.3 N m^{-2}). The binding energies of O 1*s*, Si 2*p*, Al 2*p*, and Zr 3*d* were referenced to the C 1*s* band at 284.6 eV. In order to obtain the XPS intensity ratio between Zr 3*d* and Si 2*p* (Al 2*p*), the normalized intensities of Zr 3*d*, Al 2*p*, and Si 2*p* were calculated by multiplying the relative area of the corresponding peaks by the sensitivity factors. The theoretical XPS intensity ratio of Zr 3*d* to Al 2*p* or Si 2*p* for a monolayer dispersion of zirconia was calculated according to the sheet model for dispersion of the catalyst particles proposed by Kerkhof and Moulijn (24), using the photoionization cross section determined by Scofield (25) and the escape depth of electrons proposed by Penn (26).

Pyridine FTIR spectra were recorded using a Brucker FT 88 spectrometer. The samples were pressed into self-supporting discs, placed in an IR cell, and treated under vacuum (10^{-6} Torr) at 673 K for 2 h. After cooling to room temperature, the samples were exposed to pyridine vapour for 3 minutes. Then, the spectra were recorded after evacuation (5×10^{-5} Torr) for 1 h at room temperature, 423, 523, and 623 K.

TABLE 1

Chemical Analysis and Texture Data of ZrO_2/Al_2O_3 Samples

Sample	ZrO_2 (wt%)	S_{BET} (m^2/g)	Pore volume (cm^3/g)
Al_2O_3	—	210	0.60
ZrO_2/Al_2O_3	2.2	200	0.59
ZrO_2/Al_2O_3	3.2	194	0.58
ZrO_2/Al_2O_3	7.5	192	0.57
ZrO_2/Al_2O_3	12.9	186	0.52
ZrO_2/Al_2O_3	17.1	182	0.53
ZrO_2/Al_2O_3	23.2	159	0.42

3. RESULTS

3.1. Textural Properties

The BET surface area and pore volume of the ZrO_2/Al_2O_3 and ZrO_2/SiO_2 samples after calcination are summarized in Tables 1 and 2, respectively. All samples show a decrease in the surface area after deposition of zirconia compared to the original supports. The pore volume of the samples also decreases. For ZrO_2/Al_2O_3 samples the BET surface gradually decreases with ZrO_2 content up to 17.1 wt% (Table 1). The loss in BET surface area is approximaly 20% for the sample containing 23.8 wt% ZrO_2. The ZrO_2/SiO_2 samples exhibit a smaller decrease in the surface area. For the sample with 28.6 wt% ZrO_2, this corresponds to about 10% (Table 2). This could be connected with the difference in the pore volume of alumina and silica supports, as the silica has higher pore volume compared to that of alumina. Consequently, the decrease in the surface area of ZrO_2/SiO_2 samples results from the pore plugging (the pores become smaller with increasing ZrO_2 content). The highest loss in the surface area for the ZrO_2/Al_2O_3 sample with 23.2 wt% is, probably, due to some blocking of the pores by ZrO_2 crystallites.

3.2. XRD Measurements

The extent of crystallization and of the crystalline phase formed depends on the amount of ZrO_2, the temperature,

TABLE 2

Chemical Analysis and Texture Data of ZrO_2/SiO_2 Samples

Sample	ZrO_2 (wt%)	S_{BET} (m^2/g)	Pore volume (cm^3/g)
SiO_2	—	310	1.01
ZrO_2/SiO_2	1.2	298	0.97
ZrO_2/SiO_2	8.9	283	0.90
ZrO_2/SiO_2	15.4	289	0.91
ZrO_2/SiO_2	18.3	285	0.88
ZrO_2/SiO_2	28.6	269	0.79

and the heating time. The XRD spectra of alumina and some ZrO_2/Al_2O_3 samples are shown in Fig. 1. The ZrO_2/Al_2O_3 samples with lower ZrO_2 content did not show any clear diffraction peak from zirconia (Figs. 1b and 1c). A small quantity of poorly crystallized zirconia giving reflections in the 2θ ranges of 25–35° appears in the ZrO_2/Al_2O_3 sample with 12.9 wt% zirconia (Fig. 1d). The peak characteristics of the tetragonal phase becomes larger when the ZrO_2 content increases. Three peaks from ZrO_2 at $2\theta \approx 30$, 50, and 60° are observed in the sample with 23.2 wt% ZrO_2 (Fig. 1f). It has been observed (27) that, as usual, the tetragonal form exists in microcrystallites at temperatures below the normal transformation temperature. Upon calcination at 973 K the quantity of the tetragonal phase decreased and this was accompanied by a corresponding increase in the monoclinic phase, indicating an increase of the x-ray crystallites' size. The asymmetry of the peak at $2\theta = 29$–32° (Fig. 1e) clearly indicates that two phases are present.

The x-ray diffractograms of ZrO_2/SiO_2 samples heated at 773 K did not show any peak for zirconia. Zirconia is either completely amorphous or composed of crystallites smaller than 4 nm. After calcination at 973 K, the sample with the highest ZrO_2 content (28.6 wt%) showed a very broad and weak peak in the 2θ range from 20° to 40°, indicative of a very low crystallinity.

3.3. XPS Measurements

The XPS technique provides valuable information on the location and distribution of the supported phase in the porous structure of the supports. The binding energies of O 1*s*, Al 2*p*, Si 2*p*, and Zr 3*d* and the atomic XPS intensity ratio between Zr and Al or Si for ZrO_2/Al_2O_3 or ZrO_2/SiO_2 samples are given in Tables 3 and 4, respectively.

TABLE 3

XPS Parameters of ZrO_2/Al_2O_3 Samples

ZrO_2 (wt%)	Binding energy (eV)		IZr 3*d*/IAl 2*p*
	Al 2*p*	Zr $3d_{5/2}$	
2.2	74.4	182.5	0.24
3.2	74.4	182.5	0.27
7.5	74.3	182.3	0.58
7.5[a]	74.4	182.4	0.58
12.9	74.4	182.1	0.97
17.1	74.3	182.1	1.41
23.2	74.6	182.1	1.75
23.2[a]	74.4	182.1	1.68

[a] Samples were calcined at 973 K.

The binding energy of the Al 2*p* photoelectrons is the same for all the ZrO_2/Al_2O_3 samples and identical to that of pure alumina at 74.4 ± 0.2 eV (Table 3). The binding energy of Zr $3d_{5/2}$ in the samples rich in zirconia, 182.1 eV, is in agreement with literature values of binding energy of Zr^{4+} in pure zirconia (28). For samples containing less ZrO_2, however, the Zr $3d_{5/2}$ binding energy is slightly higher (Table 3). The binding energy of Si 2*p* (103.2–103.4 eV) in ZrO_2/SiO_2 samples is smaller than that of pure silica (103.8 eV) (Table 4). The binding energy of zirconium increases (from 182.6 to 183.1 eV) with decreasing ZrO_2 loading. When the ZrO_2/SiO_2 samples containing 8.9 and

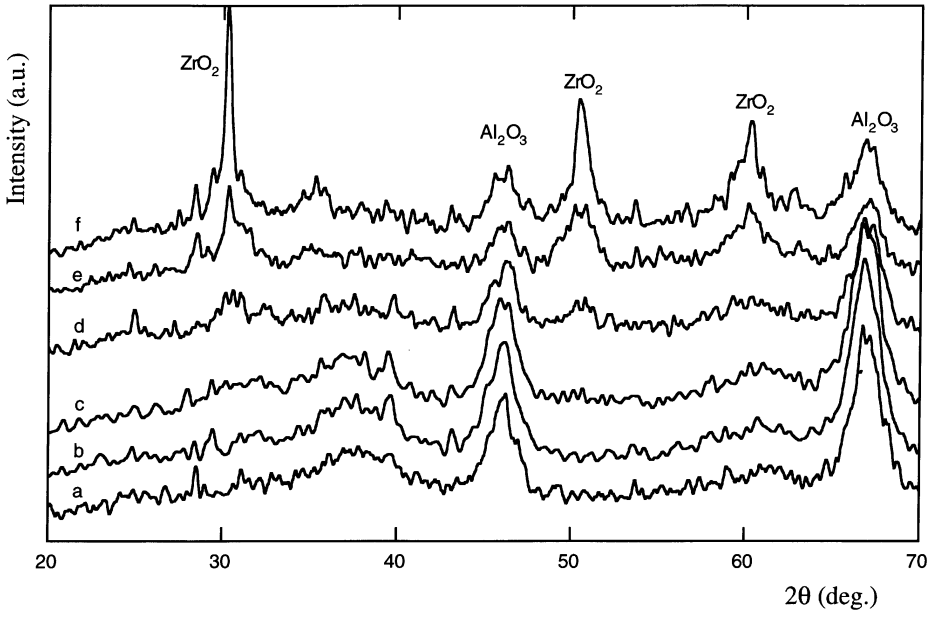

FIG. 1. X-ray diffraction patterns of (a) alumina and some ZrO_2/Al_2O_3 samples with different ZrO_2 content: (b) 3.2 wt%; (c) 7.5 wt%; (d) 12.9 wt%; and (e, f) 23.2 wt%. Spectra e are obtained at 973 K.

TABLE 4

XPS Parameters of ZrO_2/SiO_2 Samples

ZrO_2 (wt%)	Binding energy (eV)				
	Si 2*p*	Zr 3$d_{5/2}$	O 1*s*	Shoulder[a]	IZr 3*d*/ISi 2*p*
1.2	103.4	183.1	532.7	—	0.08
8.9	103.4	182.9	532.4	530.5	0.67
8.9[b]	103.3	183.1	532.6	530.9	0.63
15.4	103.2	182.8	532.4	530.6	1.20
18.3	103.2	182.7	532.4	530.5	1.48
28.6	103.2	182.6	532.6	530.6	2.70
28.6[b]	103.4	182.8	532.4	530.5	2.46

[a] Shoulder peak presented in O 1*s* spectrum.
[b] Samples calcined at 973 K for 7 h.

28.6 wt% ZrO_2 were calcined at 973 K for 7 h, there was an increase in the binding energy of Zr 3*d* photoelectrons compared to that of pure zirconia.

The theoretical and experimental XPS values of IZr 3*d*/IAl 2*p* or IZr 3*d*/ISi 2*p* as a function of the atomic ratio between Zr and Al or Si in bulk are plotted in Figs. 2A and 2B. For ZrO_2/Al_2O_3 the experimental points for samples containing less than 17.1 wt% ZrO_2 are on the straight line corresponding to a theoretical monolayer (Fig. 2A). But, when the ZrO_2 content is increased beyond this value, the experimental points fall notably below the theoretical line.

For ZrO_2/SiO_2 samples a better linear relation between the experimental XPS intensity ratios and the bulk Zr/Si composition is observed (Fig. 2B). Only a slight deviation from the theoretical line is observed at the highest concentration of ZrO_2.

3.4. FTIR Measurements

3.4.1. Basic IR Spectra

A broad absorption was observed in the OH-stretching region (4000–3500 cm^{-1}) of the alumina support. The alumina spectrum in this region is generally dominated by an intense symmetric peak at 3730 cm^{-1}, characteristic of isolated hydroxyl groups on alumina (20). The absorption bands became difficult to detect or totally obscured with increasing ZrO_2 content. No clear peak from bulk ZrO_2 could be clearly detected because the AlOH and ZrOH stretching bands are expected to be in almost the same frequency range. In particular, bands of crystalline bulk zirconia have been detected at 3740 and 3680 cm^{-1} due to terminal and bridging hydroxyl groups, respectively (30). Therefore, clear conclusions with respect to the change of OH-absorption bands of the ZrO_2/Al_2O_3 samples cannot be given.

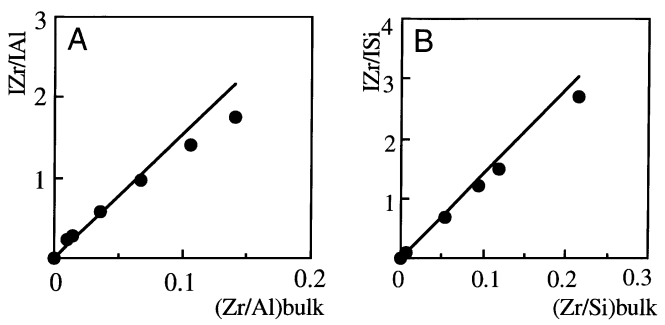

FIG. 2. Calculated (—) and experimental (●) XPS intensities for (A) ZrO_2/Al_2O_3 and (B) ZrO_2/SiO_2 samples.

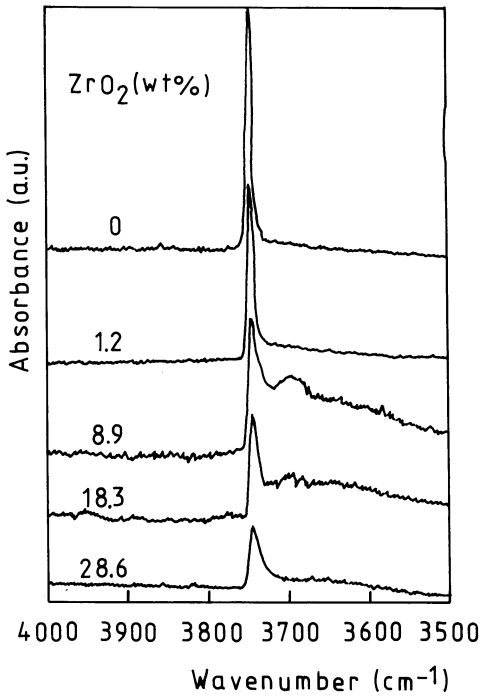

FIG. 3. Infrared spectra in the range of hydroxyl groups observation for silica and ZrO_2/SiO_2 samples with different ZrO_2 content.

The IR spectra in the OH-stretching region (4000–3500 cm^{-1}) of silica and zirconia-silica samples before exposure to pyridine are presented in Fig. 3. The difference between the spectra of the samples and support is obvious. The silica spectrum (Fig. 3) is dominated by an intense band at 3746 cm^{-1} due to isolated noninteracting surface SiOH groups (29). In the spectrum of zirconia there was a broad band in the range 3770–3600 cm^{-1} characteristic of the tetragonal and/or monoclinic phases (30). After ZrO_2 deposition, the OH-region of the spectra changed as can be seen from Fig. 3. All the ZrO_2/SiO_2 samples displayed the isolated silanol peak but with reduced intensity relative to pure silica. This fact shows that the hydroxyl groups of silica are involved in the reaction with zirconium *n*-propoxide. Bands due to OH groups of crystalline bulk zirconia at about 3740 and 3680 cm^{-1} were not detected.

3.4.2. Pyridine Adsorption

3.4.2.1. ZrO_2/Al_2O_3 samples. The infrared spectra of pyridine adsorbed on the samples in the spectral region 1700–1300 cm^{-1} give information about the type of acid sites and site strength distribution present in the different samples. According to (31) pyridine is bound to the surface in two different modes, 19b and 8a, depending on the nature of the intermolecular interactions via the nitrogen lone pair electrons. These two modes are observed at 1447–1440 and 1600–1580 cm^{-1}, respectively, for hydrogen-bonded pyridine, at 1550–1535 cm^{-1} and about 1640 cm^{-1} for the pyridinium ion. Pyridine coordinatively bonded to Lewis acid sites gives bands at 1464–1447 cm^{-1} (ν19b) and 1634–1600 cm^{-1} (ν8a). The wavenumber of the former is sensitive to the strength of the Lewis acidity, while the intensity of the latter characterizes the number of such sites.

The IR spectra of pyridine adsorbed on Al_2O_3 and ZrO_2/Al_2O_3 samples after desorption at two different temperatures (293 and 423 K) are shown in Fig. 4. Adsorption peaks at 1623, 1613, 1578, 1491, and 1498 cm^{-1}, which were all attributed to pyridine adsorbed on the Lewis acid sites, are observed on alumina after evacuation at 293 K. The smallest peak at 1593 cm^{-1} was assigned to pyridine bonded to the OH groups on the Al_2O_3 surface. In addition to the bands observed for alumina, a new band appears at about 1607 cm^{-1} in the spectra of ZrO_2/Al_2O_3 (Fig. 4a). This is assigned to acidity generated from the presence of zirconia. On zirconia, pyridine adsorption was characterized by a band at 1613 cm^{-1}. The relative proportion between the two types of Lewis acid sites, the weak one at 1609 cm^{-1} and the stronger at 1623 and 1613 cm^{-1}, depends on the composition of the samples. At the highest ZrO_2 content the intensity of the weak Lewis acid sites increases relative to the strong ones. After heating of the samples at 423 K some shift to higher wavenumbers and a decrease in the intensity of the bands is observed (Fig. 4b). The FWHM (full width of half maximum) is also modified and decreases when increasing the evacuation temperature. The band at 1593 cm^{-1} from weakly bonded pyridine disappears. In the spectra of all the samples a splitting of the 19b band, at 1455 and 1452 cm^{-1}, is observed, indicating that different types of acid sites are formed. It can be noted that after evacuation at the highest temperature (623 K) peaks at 1624 and 1456 cm^{-1} are present in the spectra of ZrO_2/Al_2O_3 samples. This indicates the presence of strong Lewis acid sites from coordinatively bonded pyridine.

In summary, two different modes of pyridine desorption from ZrO_2/Al_2O_3 can be observed: one which takes place up to 423 K and is assigned to H-bonded and coordinated pyridine and another one, at higher temperatures (523 and 623 K), corresponding to singly coordinated pyridine.

Figure 5 shows the change in the relative total number of Lewis acid sites per gram with ZrO_2 content (given by the area of the 19b band at 1464–1447 cm^{-1} taken after

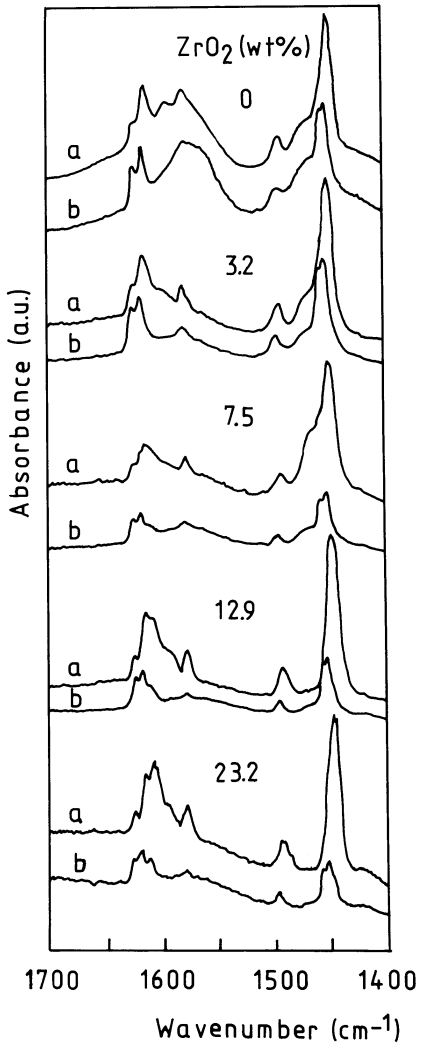

FIG. 4. Infrared spectra of pyridine after desorption at (a) 298 and (b) 423 K on ZrO_2/Al_2O_3 samples with different ZrO_2 content.

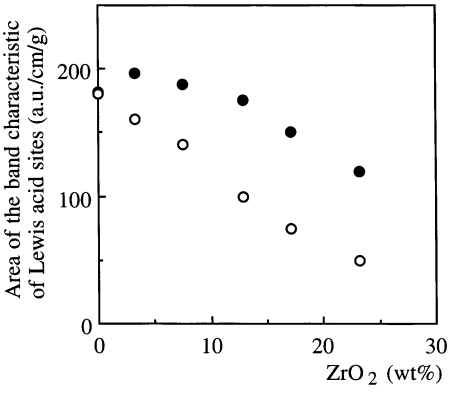

FIG. 5. Variation of the area of the bands characteristic of the total number of Lewis acid sites (●) and the strong Lewis acid sites (○) in ZrO_2/Al_2O_3 samples.

evacuation of pyridine at 423 K). The number of Lewis acid sites increases slightly at the lowest ZrO_2 content (3.2 wt%) but decreases with a further increase of ZrO_2. The area of the bands specific for the strong Lewis acid sites has also been determined by decomposition of the spectra in the 1650–1600 cm^{-1} frequency range. Its variation with zirconia content is also presented in Fig. 5. It decreases with ZrO_2 content due to the formation of ZrO_2 crystallites, generating weak acid sites.

3.4.2.2. ZrO_2/SiO_2 samples. The IR spectra of pyridine adsorbed at room temperature on SiO_2 and ZrO_2/SiO_2, after evacuation at two different temperatures, are shown in Fig. 6. When pyridine is evacuated at 293 K from a silica sample only two infrared bands at 1597 and 1446 cm^{-1} due to hydrogen bonded pyridine are observed. These bands disappeared after evacuation at 423 K, thus reflecting a relatively weak surface acidity. On zirconia, pyridine adsorption

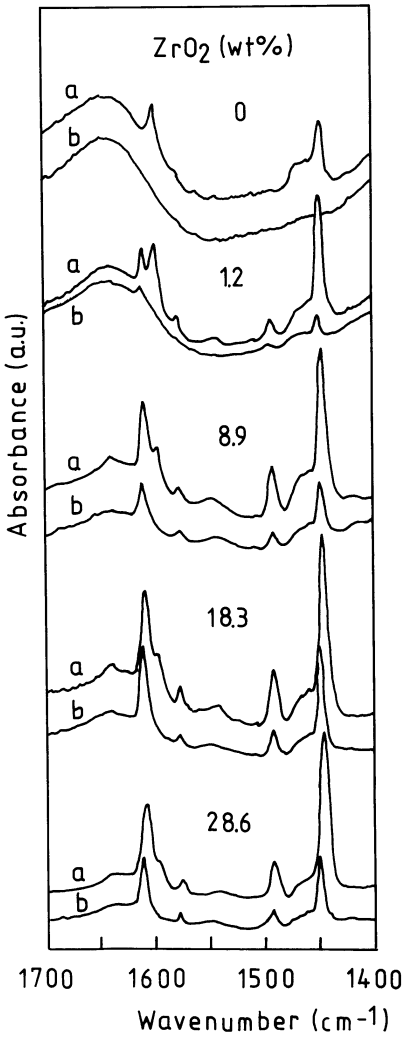

FIG. 6. Infrared spectra of pyridine after desorption at (a) 298 and (b) 423 K on ZrO_2/SiO_2 samples with different ZrO_2 content.

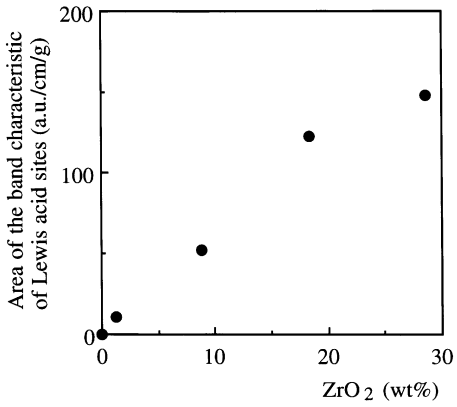

FIG. 7. Variation of the area of the bands characteristic of the total number of Lewis acid sites with ZrO_2 content in ZrO_2/SiO_2 samples.

was characterized by a band at 1613 cm^{-1}. The strong bands of coordinatively bonded pyridine at 1610 and 1447 cm^{-1} (along with the band from silica at 1597 cm^{-1} and bands at 1577 cm^{-1} and 1491 cm^{-1} due to H-bonded pyridine) appear in the spectra of all the ZrO_2/SiO_2 samples after evacuation at room temperature (Fig. 6a). Quite a weak band corresponding to some Brønsted acid sites appeared at about 1545 cm^{-1} (ν19b). The desorption of pyridine at 423 K led to a decrease in the band intensity, especially of the 1577 and 1491 cm^{-1} bands, in all samples (Fig. 6b) and shifted the 8a and 19b bands to 1610–1612 and 1449 cm^{-1}, respectively. The intensity of the bands of Brønsted acidity was also reduced. All adsorbed pyridine was removed after evacuation at 523 K. Figure 7 indicates that the total number of Lewis acid sites increases as the ZrO_2 content in the ZrO_2/SiO_2 samples grows.

4. DISCUSSION

4.1. Morphology and Dispersion of Zirconia

It has been shown by Kerkhof and Moulijn (24) that for monolayer catalysts a linear relation between the theoretical XPS intensity (given by the model) and the bulk atomic ratio existed with increasing content of the deposited component on the support surface. Let us first consider the state of the zirconia layer on Al_2O_3. The experimental XPS IZr 3*d*/IAl values correspond to a monolayer dispersion up to 12.9 wt% (Fig. 2A), and no XRD peaks corresponding to the ZrO_2 phase are observed. This is no longer the case for 17.1 and 23.2 wt% ZrO_2. In addition, the loss in the specific surface area seems to be substantially more important above 17.1 wt%. We therefore conclude that for ZrO_2 contents up to the range 12.9–17.1 wt% ZrO_2 (and probably close to the upper value) zirconium is atomically dispersed on Al_2O_3. Above 17.1 wt% crystallites of tetragonal ZrO_2 are formed and some pores are probably closed by such crystallites.

In the case of silica, the increase in the experimental XPS IZr 3*d*/ISi indicates that ZrO_2 appears as a monolayer close to full coverage (near 28.6 wt%) (Fig. 2B). At 28.6 wt% ZrO_2 some deviation from the proportionality between surface and bulk Zr/Si ratio begins to appear. The fact that a good dispersion is observed is also confirmed by the XRD spectra of the samples; no ZrO_2 crystallites are detected. For this reason we can say that the majority of ZrO_2 at this concentration forms a monolayer on the silica surface and a very small part of the zirconium plugs the pores. This interpretation is confirmed by the conclusions of Kerkhof and Moulijn (24).

Comparing the obtained results with those published by Dang *et al.* (19), we must conclude that our ZrO_2/SiO_2 samples have a higher dispersion. Those authors studied some silica-supported zirconia samples which had been prepared by impregnation of silica with zirconyl nitrate. They detected the monoclinic phase of ZrO_2, which grew in intensity when the ZrO_2 loading was increased from 5 to 20 wt%.

Marquez-Alvarez *et al.* (20) prepared ZrO_2/SiO_2 samples by deposition of zirconium tetra-tert-butoxide using acetylacetone in the precursor mixture. Contrary to our observations, they observed that the zirconium to silicon or aluminium XPS intensity ratios for samples with the same ZrO_2 content prepared by slightly different methods (different solution) decreased when zirconia becomes better dispersed. Their arguments are based on the uniform distribution of zirconia within the pores of the support and was difficult to detect by XPS technique.

4.2. Interaction between Zirconia and Support

4.2.1. ZrO_2/Al_2O_3 Samples

The slight increase in the BE of Zr $3d_{5/2}$ photoelectrons for samples with lower ZrO_2 content compared to that of pure zirconia (Table 3) would be connected with some change in the coordination number of zirconium. The same has been observed for other systems (32). This could be explained by an interaction of Zr with Al atoms due to formation of a Zr–O–Al bond.

A comparison of the XR diffraction peaks in the 2θ ranges of 43–49° and 65–70° in the spectra of the ZrO_2/Al_2O_3 samples with those of the samples with alumina support shows a change in the intensity and the shape of the peaks, depending on the ZrO_2 content and calcination temperature (Fig. 1). At 3.2 and 7.5 wt% ZrO_2, a small change in the Al_2O_3 XRD peaks is observed (Figs. 1a–1c). The significant decrease in the intensity of the alumina peak after 12.9 wt% ZrO_2 could be explained by (i) the presence of some interaction between zirconia and alumina and (ii) covering of the alumina support by ZrO_2 crystallites. This is more evident after calcination at higher temperature (973 K) for a long time (7 h) (Figs. 1d–1f).

The fact that the total number of Lewis acid sites in the samples with low zirconia content remains close to that of alumina (Fig. 5) leads us to believe that some substitution of aluminium atoms by zirconium at lower zirconia loadings is possible. The number of acid sites begins to decrease at higher concentration, when ZrO_2 crystallites are clearly detected by XRD.

4.2.2. ZrO_2/SiO_2 Samples

4.2.2.1. XPS. Because clear evidence of an interaction between zirconia and silica exists, we shall discuss in some detail the corresponding XPS results. A conspicuous observation is a shift in the binding energy of Zr $3d_{5/2}$ photoelectrons in the range of 0.5–1 eV for ZrO_2/SiO_2 samples compared to pure ZrO_2 (182.1 eV). A priori, this could be assigned to an atomic dispersion of zirconia on the support and/or the change in the coordination number of zirconium by formation of a Zr–O–Si bond. The decrease in BE of Si 2*p* relative to that in pure silica is also indicative of some interaction between Zr and Si atoms. A similar effect has been observed for titania-coated silica samples when titania is in close interaction with the support (32). The shift in the binding energy of titanium has been attributed principally to the changes in the coordination numbers of titanium from sixfold coordinated to oxygen in anatase to fourfold coordinated to oxygen in Ti–O–Si, i.e., when Ti^{4+} is predominantly substituted for Si in the tetrahedrally coordinated sites (32).

The slight decrease in the XPS IZr 3*d*/ISi 2*p* ratio upon calcination at higher temperature suggests that zirconia then undergoes a stabilization on the support surface due to a strong interaction between silica and zirconium, preventing the degree of sintering of zirconium particles.

An additional experiment permits us to bring additional light on these results and interpretation. For this, we compare the XPS O 1*s* lines of a ZrO_2/SiO_2 sample containing 8.9 wt% ZrO_2 with a mechanical mixture of SiO_2 with 10 wt% ZrO_2. The O 1*s* spectrum of the mechanical mixture, presented in Fig. 8a, consists of two well defined peaks, and the difference between their binding energies is 3 eV. The binding energy of 533 eV of the dominant peak is characteristic of O^{2-} in SiO_2. That of 529.9 eV of the smaller peak is assigned to the Zr–O bond in pure ZrO_2. On the other hand, the O 1*s* peak of ZrO_2/SiO_2 samples was not symmetric, but presented a shoulder (Fig. 8b). The intensity of the shoulder peak increases with increasing ZrO_2 component. Decomposition of the O 1*s* photoelectron line of the samples gives one peak at 532.5 eV which would correspond to the oxygen near a Si atom in SiO_2 and another one which is more than 0.6 eV higher than that corresponding to the oxygen in ZrO_2 (Table 4). This suggests that the low binding energy component of the O 1*s* line originates from the presence of a new type of oxygen group due to the interaction between zirconium and silica suggested above.

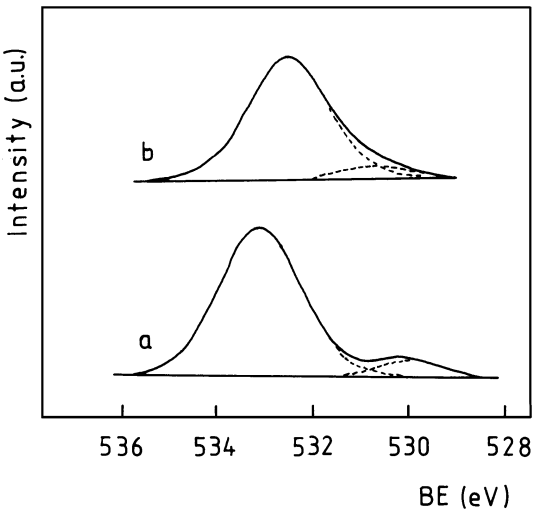

FIG. 8. XPS spectra of the O 1*s* lines of (a) the mechanical mixture ($SiO_2 + 10$ wt% ZrO_2) and (b) the ZrO_2/SiO_2 sample with 8.9 wt% ZrO_2.

The new binding energy of 530.5–530.9 eV (Table 4) may be attributed to the Zr–O–Si bond. It seems that this change is close to the change in the coordination number of zirconium or to the electron charge on zirconium atoms. This will be discussed later.

4.2.2.2. Acidity. We may expect that the observed interaction between zirconium and silicon in ZrO_2/SiO_2 would make the corresponding samples behave differently from ZrO_2/Al_2O_3. In particular, the surface acidity would reflect this influence. The generation of new acid sites in ZrO_2/SiO_2 samples is easily understood when considering the change in the binding energies of Zr 3*d* and O 1*s* photoelectrons (Table 4) which reflects modifications of the charge on the atoms. The higher binding energy of O 1*s* of the oxygen near Zr atoms compared to that in pure ZrO_2 is indicative of a lower electron density on the oxygen atoms. On the other hand, the shift in the binding energy of Zr $3d_{5/2}$ to higher values with decreasing ZrO_2 content in comparison with that for pure zirconia indicates a higher positive charge on Zr atoms. The increase in the positive charge on zirconium corresponds to the creation of Lewis acid sites. The same has been found by Slinkin *et al.* in mixed ZrO_2/SiO_2 oxides (33).

The shift in the binding energies of O 1*s* near Si atoms and Si 2*p* (Table 4) could be explained by a very small decrease in the positive charge of Si atoms and a higher electron density of the oxygen atom. This leads to the formation of some Brønsted acid sites according to the observations of Barr *et al.* (34) and Okamoto *et al.* (35). On studying the surface chemistry of zeolites by ESCA, these authors found that the binding energies of both Si 2*p* and O 1*s* are lower when the Si/Al ratio decreases. The latter suggests an increase in the covalent character of the Si–O bond, and consequently, an increase in the number of Brønsted acid sites.

These XPS findings correlate well with the IR results which gives evidence for the presence of Lewis acid sites as well as the weaker Brønsted acid sites on the surface of the ZrO_2/SiO_2 samples. Since zirconium is supposed to be responsible for the Lewis acidity, the number of Lewis acid sites for these samples should be proportional to, or at least increase with, the number of the exposed Zr attoms (as silica possesses only a very weak Lewis acidity). In reality, due to the covalency of the silica support, the condensation of the surface hydroxyl groups into water and coordinatively unsaturated cations is difficult. The consequence would be that the number of very strong Lewis acid sites is very small. Correlatively, the Lewis acid sites present in the samples would correspond mainly to weaker Lewis acid sites.

It is interesting to compare our characterization study with the models postulated in the literature on the generation and nature of the acid sites. In general, both models, those of Tanabe *et al.* (36) and Fung (37), attract attention. It is important to note that these models have been applied to chemical mixed oxides, i.e., when cationic substitution takes place in the host matrix. The central feature of the Tanabe acidity model (36) is the presence of an excess of negative or positive charge at the site of the minor component cation which generates Brønsted and Lewis acidity, respectively. The model postulates a heterolinkage in which the cations retain their coordinations while oxygen atoms adopt the coordination of the oxygens of the major component. According to the model of Kung (37) the resulting acidity in the mixed oxides depends on the difference in the ionicity or covalency of the single oxide. Bosman *et al.* (38) have observed a correlation between the electronegativity of the components and the acidity in the mixed ZrO_2/SiO_2 oxides. They interpreted the observed strong Lewis acidity as due to the high electronegativity of the Zr^{4+} cation incorporated in a more covalent SiO_2 matrix. Their argument is based on the fact that the Zr^{4+} cation is the most ionic component in the system acoording to the electronegativity scale of Pauling ($x = 10.1$ for Zr^{4+} and $x = 12.1$ for Si^{4+} (38)).

In our opinion, the model of Kung better fits our systems. Similar to the acidity generation in the mixed ZrO_2/SiO_2 oxides (38), the Lewis acid sites in our samples can also be a consequence of the higher ionicity of the Zr–O bond. This confirms that the presence of these sites is connected to the positive charge of the zirconium atoms, as shown by the increase in the binding energies of Zr 3*d* (Table 4).

Concerning the Brønsted acid sites, different types of corresponding acidity are generated in the mixed oxides. According to the model of cationic Brønsted acid sites (39), zirconium should be incorporated into the tetrahedral structure of silica to produce a labile proton. Contrary to the ability of titanium in TiO_2/SiO_2 mixed oxides to adopt the

tetrahedral coordination in the silica network it has been shown that zirconium does not enter the tetrahedral coordination of the silica network at any composition and prefers a coordination of 6, 7, or 8 (40).

The second type of Brønsted acidity denoted as being of anionic type (39) is produced by atoms which form highly electronegative anions. The model is the following: the electron density of the OH bonds is reduced by the inductive effects of the nearby electronegative anions; this weakens the OH bond and generates a Brønsted acidity. The latter is in accordance with Kung's assumptions that (i) an electrostatic interaction exists between two components and (ii) Zr–O bonds neighboring the more covalent Si–O units possess a higher ionicity. The same effect has been observed by Yamaguchi *et al.* (41) and Kawai *et al.* (42) for ZrO_2/SiO_2 systems prepared by impregnation of SiO_2 with $Zr(n\text{-}OC_3H_7)_4$. In a study of the surface electron structure of the samples, these authors have shown that the Brønsted acidity can be formed by the charge transfer from a ZrO_4 unit to the SiO_4 unit, namely that the Si–O bond of Si tetrahedra and neighboring Zr tetrahedra became stronger and the acidity of H^+ on SiOH also became stronger. We believe that the Brønsted acid sites in our ZrO_2/SiO_2 samples can be formed allowing the same mechanism as that proposed by Kung. Observing the increase of the electron density on the oxygen present in the Si–O bond, we would propose that acidic hydroxyls are formed on the surface of SiO_2.

In summary, the present study confirms that the above ideas about the acidity generation in the mixed oxides could be applied to our systems. Although our oxides are not true mixed oxides, being prepared by impregnation of SiO_2 by zirconium alkoxide, the results clearly show that in parallel to Lewis acidity generation, there are some surface regions where Zr–O–Si bonds of strength sufficient to protonate pyridine are generated. This is an indication that a strong interaction exists between the support and deposited zirconium, and makes this system similar to chemically mixed oxides.

5. CONCLUSIONS

It is found that the surface reaction of alumina and silica with zirconium *n*-propoxide leads to high dispersion. This dispersion depends on several parameters such as the type of the support, heating treatment, and zirconia content.

The type of the support and zirconia content strongly influences the morphology and dispersion of zirconia. Zirconia on alumina is atomically dispersed and forms a monolayer in the range 12.2–17.1 wt% ZrO_2. After this concentration ZrO_2 crystallites are formed. On silica zirconia is amorphous at all ZrO_2 contents. ZrO_2 appears as a monolayer until there is almost full silica coverage (near 28.6 wt%).

There is a strong interaction between Zr and Al(Si) atoms due to formation of Zr–O–Al(Si) bonds. The degree of the Zr–O–Al bond decreases with the ZrO_2 content. The strong Zr–O–Si bond in the ZrO_2/SiO_2 samples leads to the generation of Lewis acid sites, detected by a higher positive charge on the Zr atoms. Some Brønsted acid sites are also observed due to an increase in the electron density on the oxygen atom at the Si–O bond.

ACKNOWLEDGMENTS

We thank the Ministre des Affaires Etrageres due Commerce Exterieres et de la Cooperation au Development (Belgium) for a NATO grant to S.D. We also thank the Fonds National de la Recherche Scientifique (Belgium) for grants for purchasing the XRD and XPS equipments.

REFERENCES

1. Tanaka, K., and Okuhara, T., *J. Catal.* **65**, 1 (1980).
2. Shima, H., and Yamaguchi, T., *J. Catal.* **90**, 160 (1984).
3. Tanabe, K., and Yamaguchi, T., *Catal. Today* **20**, 185 (1994).
4. Yamaguchi, T., Sasaki, H., and Tanabe, K., *Chem. Lett.*, 1077 (1973).
5. Davis, B. H., *J. Catal.* **79**, 58 (1983).
6. Yamaguchi, T., Nakano, Y., Iizuka, T., and Tanabe, K., *Chem. Lett.*, 1053 (1976).
7. Daly, F. P., Ando, H., Schmitt, J. L., and Sturm, E. A., *J. Catal.* **108**, 401 (1987).
8. Tanabe, K., *Mater. Chem. Phys.* **135**, 347 (1985).
9. Tanabe, K., Misono, M., Ono, Y., and Hattori, H., *Stud. Surf. Sci. Catal.* **51**, 1 (1989).
10. Yamaguchi, T., *Appl. Catal.* **61**, 1 (1990).
11. Arata, K., *Adv. Catal.* **37**, 165 (1990).
12. Riemer, T., Spielbauer, D., Hunger, M., Mekhemer, G. A. H., and Knozinger, H., *J. Chem. Soc., Chem. Commun.*, 1181 (1994).
13. Kustov, L. M., Kazansky, V. B., Figueras, F., and Tichit, D., *J. Catal.* **150**, 143 (1994).
14. Corma, A., Formes, V., Jvan-Rajadell, M. I., and Lopez-Nieto, J. M., *Appl. Catal. A: General* **116**, 151 (1994).
15. Ward, D. A., and Ko, E. I., *J. Catal.* **150**, 18 (1994).
16. Amenomiya, Y., *Appl. Catal.* **30**, 57 (1987).
17. Ghiotti, G., Chiorino, A., and Boccuzi, F., *Surf. Sci.* **251**, 1100 (1990).
18. Meijers, A. C. Q. M., Jong, A. M., van Grujthreijsen, L. M. P., and Niemantserdriet, J. W., *Appl. Catal.* **70**, 53 (1991).
19. Dang, Z., Anderson, B. G., Amenomiya, Y., and Morrov, B. A., *J. Phys. Chem.* **99**, 14437 (1995).
20. Marquez-Alvarez, C., Fierro, J. L. G., Guerrero-Ruiz, A., and Rodriguez-Ramos, I., *J. Colloid. Interface Sci.* **159**, 454 (1993).
21. Shane, M., and Mecartney, M., *J. Mater. Sci.* **25**, 1537 (1990).
22. Debsikdar, J. C., *J. Non-Cryst. Solids* **86**, 231 (1986).
23. Eshelman, L. M., de Jong, A. M., and Niemantsverdriet, J. W., *Catal. Lett.* **10**, 201 (1991).
24. Kerkhof, F. P. J. M., and Moulijn, J. A., *J. Phys. Chem.* **83**, 1612 (1979).
25. Scofield, J. H., *J. Electron Spectrosc. Relat. Phenom.* **8**, 129 (1976).
26. Penn, D. R., *J. Electron Spectrosc. Relat. Phenom.* **9**, 29 (1976).
27. Garvie, R. C., *J. Phys. Chem.* **69**, 1238 (1965).
28. Morant, C., Sanz, J. M., Galan, L., Soriano, L., and Kueda, F., *Surf. Sci.* **218**, 331 (1989).
29. Morrow, B. A., and McFarlan, A. J., *Langmuir* **7**, 1695 (1991).
30. Yamaguchi, T., Nakano, Y., and Tanabe, K., *Bull. Chem. Soc. Jpn.* **51**, 2482 (1978).
31. Morterra, C., and Cerrato, G., *Langmuir* **6**, 1810 (1990).
32. Castillo, R., Koch, B., Ruiz, P., and Delmon, B., *J. Mater. Chem.* **4**, 903 (1994).

33. Slinkin, A. A., Klyachko, A. L., Shpiro, E. S., Kapustin, G. I., Kucherova, T. N., Stakneev, A. Yu., and Ermolov, L. V., *Kinet. Katal.* **32**, 725 (1991).
34. Barr, T. L., and Lishka, M. A., *J. Am. Chem. Soc.* **108**, 3178 (1986).
35. Okamoto, Y., Ogawa, M., Maezawa, A., and Imanaka, T., *J. Catal.* **112**, 427 (1988).
36. Tanabe, K., Sumiyoshi, T., Shibata, K., Kiyoura, T., and Kitagawa, J., *Bull. Chem. Soc. Jpn.* **47**, 1064 (1974).
37. Kung, H. H., *J. Solid State Chem.* **52**, 191 (1984).
38. Bosman, H. J. M., Pijpers, A. P., and Jaspers, A. W. M. A., *J. Catal.* **161**, 551 (1996).
39. Connell, G., and Dumesic, J. A., *J. Catal.* **105**, 285 (1987).
40. Bihuniak, P., and Condrate, P., *J. Non-Cryst. Solids* **44**, 331 (1981).
41. Yamaguchi, T., Morita, T., Salena, T. M., and Tanabe, K., *Catal. Lett.* **4**, 1 (1990).
42. Kawai, M., Tsukada, M., and Tamaru, K., *Surf. Sci.* **111**, L716 (1981).